



Effects of forging parameters on uniformity in deformation and microstructure of AZ31B straight spur gear

Zhao-yang JIN¹, Nan-nan LI¹, Qi ZHANG¹, Kai YAN¹, Zhen-shan CUI²

1. College of Mechanical Engineering, Yangzhou University, Yangzhou 225127, China;

2. National Die and Mold CAD Engineering Research Center, Shanghai Jiao Tong University, Shanghai 200030, China

Received 28 November 2016; accepted 25 May 2017

Abstract: The effects of forging parameters on the deformation and microstructure distributions of as-forged straight spur gears were investigated by finite element (FE) simulation and statistical analysis method. Spur gear forging using the movable cavity die design was investigated by integrating the FE method with the microstructure evolution models for AZ31B magnesium alloys. The required inputs such as flow stress curves and microstructure evolution models, were obtained through the Gleeble thermal mechanical testing and quantitative metallography analysis method. Numerical simulation and experimental examination confirm that both the deformation and microstructure are non-uniformly distributed in the as-forged gears. Decreasing deformation temperature or increasing strain rate is beneficial to obtaining fine-grained microstructure but is harmful to the uniformity in deformation or microstructure. The level of the non-uniformity results from the complex shape of gear and the friction between the billet and dies, which is closely associated with the characteristics of flow stress curve.

Key words: magnesium alloys; straight spur gear; hot forging; finite element method; microstructure evolution

1 Introduction

Straight spur gears are typical transmission component, which are widely used in automobiles and kinds of machinery parts. The conventional method to produce straight spur gears is cutting. Compared with cutting, forging is of high material utilization, high productivity and low cost. Furthermore, continuous, dense and uniform metal streamline observed in the as-forged gear results in significantly improved mechanical properties. As one of the main net-shape or near net-shape forming technologies, precision forging has successfully been used to manufacture spur bevel gears. However, forming a qualified straight spur gear through precision forging is technically difficult, for example, filling metal in tooth corner completely and reducing forging load. To resolve those difficulties, TUNCER and DEAN [1] proposed an idea of movable cavity die design, in which the friction was designed to assist in improving forming quality and in lowering forming load. Since then, new ideas of spur gear

precision forging, various relief-hole and alternative-die designs for instance, have been proposed to improve the forming quality [2–4]. In recent years, finite element method (FEM) has been applied to analyzing the effect of billet geometry, die design and processing parameters on precision forging of spur gears or helical gears [5,6]. These studies mainly focus on metal filling and deformation fields of as-forged gears but not on the microstructure evolution.

For AZ31B magnesium alloys with low-medium stacking-fault energy, dynamic recrystallization (DRX) occurs during hot deformation process. On one hand, microstructure changes as a result of DRX alter the mechanical properties of the alloy such as flow stress, and then affect the subsequent deformation process; on the other hand, deformation behavior influences the microstructure evolution in reverse. Therefore, optimizing microstructure through adjusting deformation parameters is an important way to improve the mechanical properties of the forgings. In recent decade, microstructure evolution during hot deformation has become a research hotspot. DONG et al [7] studied the

homogeneity of microstructure and hardness in cold closed-die forged gears of 20CrMnTi alloy by experimental measurements. ZHANG et al [8] applied the finite element method to investigate the metal flow of aluminum alloys undergoing the porthole die extrusion, and the oxide distribution in longitudinal and transverse welding zones was measured by scanning electron microscopy and optical microscopy. WANG et al [9] established the DRX kinetics on the basis of thermal mechanical testing and metallography examination. Some researchers integrated the microstructure evolution models with finite element model to simulate the microstructure evolution of hot-compressed cylindrical samples made of steel [10], magnesium alloys [11], titanium alloys [12] and nickel-based superalloys [13]. This micro-macro coupled model was also applied to simulating the microstructure evolution of a special-shaped components such as forged pipes [14,15] and hot rolling plates [16]. However, rare numerical simulations are found to investigate the microstructure evolution of complex-shaped forged straight spur gears.

In this work, forging process of AZ31B straight spur gear was studied by developing a thermal-mechanical-microstructural coupled finite element model, and the die structure was designed based on the principle of friction-assisted tooth filling. The effects of deformation parameters on the uniformity of deformation and microstructure were studied and a trial forging was carried out to verify the established model.

2 Finite element model for hot forging of AZ31B straight spur gears

2.1 Flow stress curves of AZ31B magnesium alloys

The flow stress curves at high temperatures required to input into the finite element model were obtained by the Gleeble thermal mechanical testing. This testing was implemented on the Gleeble-1500 machine for the commercial extruded-AZ31B magnesium alloys, which was chosen as the billet material for forging gears. During testing, the cylindrical specimen, with the sizes of $d10\text{ mm} \times 15\text{ mm}$, was heated to the deformation temperature at a rate of $5\text{ }^{\circ}\text{C/s}$, held for 5 min at the temperatures of 250, 300, 350 and $400\text{ }^{\circ}\text{C}$ to avoid the temperature gradient in the specimen, and then compressed at strain rates of 0.001, 0.01, 0.1 and 1 s^{-1} till the true strain reaches 0.9. Figure 1 shows the true stress-strain curves of AZ31B alloys obtained by the experiments.

2.2 Microstructure evolution models of AZ31B magnesium alloys

In order to preserve the deformation microstructure at elevated temperatures, the specimen was quenched in

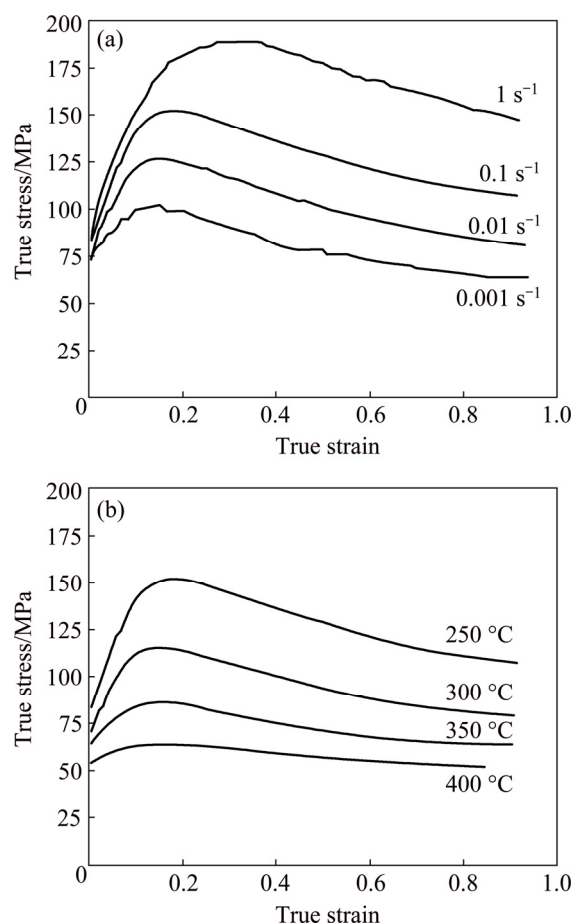


Fig. 1 True stress-strain curves of AZ31B alloys obtained at temperature of $250\text{ }^{\circ}\text{C}$ (a) and strain rate of 0.1 s^{-1} (b)

water immediately after the Gleeble testing. Then, this specimen would be cut off through the axis line along the compression direction. After being polished, the cross section was etched for 10–15 s by the mixed solution of oxalic acid, nitric acid and acetic acid. Dynamic recrystallized grain size determined by the quantitative metallographic analysis was obtained over 10 fields of view by the Leica DMI 3000M optical microscope. The least squares method was applied to obtaining the microstructure evolution models for the pre-extruded AZ31B magnesium alloys. As expressed in Eq. (1), the average grain size (D_{avg}) in the deformation zone is dependent on the initial grain size (D_0), DRX grain size (D_{DRX}) and DRX volume fraction (x). The value of D_{DRX} is a function of the Zener-Hollomon parameter (Z) as expressed in Eqs. (2) and (3). Considering the co-occurrence of deformation and DRX during hot deformation, it is difficult to distinguish the recrystallized grain from the non-recrystallized matrix, so, the value of x is difficult to be figured out accurately through the metallographic examination. However, the macroscopic flow stress curve exhibits the information on internal microstructure evolution, so, the value of x can be obtained instead from the hardening and softening

characteristics of measured flow stress curves, as shown in Eqs. (4)–(6) [13,17].

$$D_{\text{avg}} = D_0(1-x) + D_{\text{DRX}} \cdot x \quad (1)$$

$$D_{\text{DRX}} = 408.2583Z^{0.1105} \quad (2)$$

$$Z = \dot{\varepsilon} \exp[Q/(RT)] \quad (3)$$

$$x = \begin{cases} 0, & \varepsilon < \varepsilon_{\text{cr}} \\ 1 - \exp\left(-0.693\left(\frac{\varepsilon - \varepsilon_{\text{cr}}}{\varepsilon_{0.5} - \varepsilon_{\text{cr}}}\right)^{1.3152}\right), & \varepsilon > \varepsilon_{\text{cr}} \end{cases} \quad (4)$$

$$\varepsilon_{\text{cr}} = 0.00178Z^{0.1380} \quad (5)$$

$$\varepsilon_{0.5} = 0.0343Z^{0.0783} \quad (6)$$

where D_0 is 22 μm in this study, $\dot{\varepsilon}$ is the strain rate, R is the mole gas constant, T is the deformation temperature, $Q=157.84$ kJ/mol is the deformation activation energy for AZ31B magnesium alloys; ε_{cr} is the critical strain for occurrence of DRX and $\varepsilon_{0.5}$ is the strain where $x=50\%$. Figure 2 presents the calculated recrystallization volume fraction curves for Gleeble samples deformed at the temperatures of 250 and 350 $^{\circ}\text{C}$ and at the strain rates of 0.001 and 1 s^{-1} . Figure 3 gives the measured average sizes of dynamic recrystallized grains under different deformation conditions. The calculated values are also given for the ease of comparison. The mean value of relative error between the experiments and the calculation is about 5.72%.

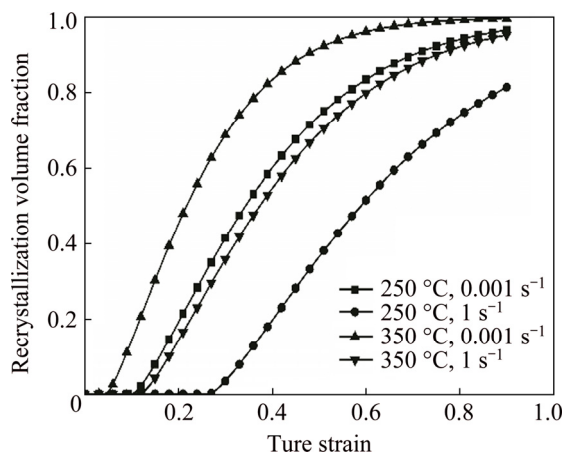


Fig. 2 Calculated recrystallization volume fraction curves for Gleeble samples deformed under different conditions

2.3 Finite element model for straight spur gears

Taking a customized straight spur gear for automobile electro-motor as an example, the die structure is based on the movable cavity die design proposed by TUNCER and DEAN [1], where friction-assisted principle is applied to improving filling and lower forming load. Figure 4 shows the schematic diagram of the designed die structure. The billet was put in the cavity of the floated toothed die. When the flat end

of the flange connected with the toothed punch contacted the flat surface of the die cavity, it pushed both the billet and the die cavity to move down. Since the direction of friction force between the billet and the toothed die is the same as that of the tooth filling, the friction force will not impede but promote the tooth filling. The parameters describing the gear geometry are shown in Table 1.

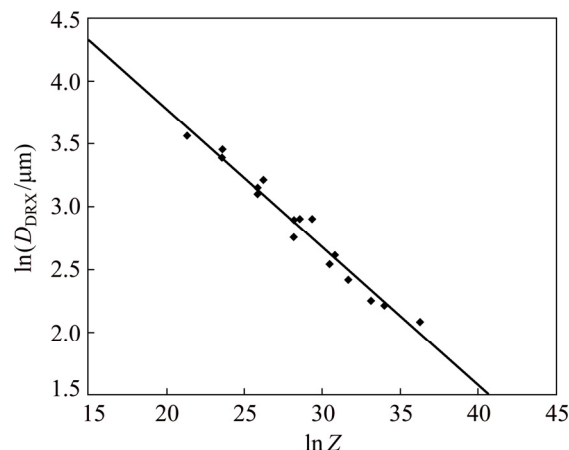


Fig. 3 Comparison between measured and calculated average sizes of DRX grain for Gleeble samples under different deformation conditions

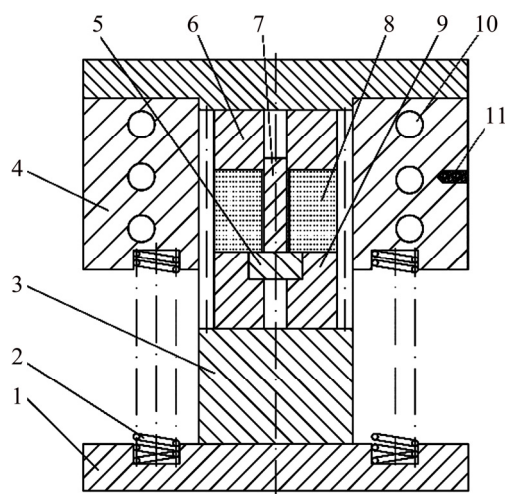


Fig. 4 Schematic diagram of movable cavity die design for straight spur gear (1—Bolster; 2—Spring; 3—Anvil; 4—Die cavity; 5—Anvil; 6—Toothed punch; 7—Mandrel; 8—Billet; 9—Toothed ejector; 10—Heating bore; 11—Thermocouple)

For the FEM simulation, the billet and the die geometry models were established in the SolidWorks software and then imported into the FEM software Msc. Marc. For the purpose of saving computational time, one tooth was taken for the FEM analysis due to the symmetry of the investigated gear. Die and the mandrel were set as a rigid body and the billet was set as elastic-plastic body. Hot forging was performed under isothermal condition. The flow stress data of AZ31B

magnesium alloys obtained from the Gleeble thermal mechanical testing were imported into the FEM model through user-defined material library, and the developed microstructure evolution models were integrated with the FEM model through the UGRAIN user-subroutine interface. The heat transfer coefficient between billet and air is set as $20 \text{ W/(m}^2\cdot\text{°C)}$, the heat transfer coefficient between the billet and the dies is $3000 \text{ W/(m}^2\cdot\text{°C)}$, and the friction coefficient between the billet and the mold is set as 0.3.

3 Simulation results and discussion

3.1 Effects of deformation parameters on effective strain distribution

Figure 5 shows the distribution of effective strain of AZ31B spur gears at the end of forging process performed at temperatures of 250 and 350 °C and strain rates of 0.001 and 1 s^{-1} . The vertical axis represents the percent of nodes at a specific level of effective strain. It is shown that the effective strains of gears forged under

different processing parameters are non-uniformly distributed. The effective strain in the area of the tooth is significantly higher than that between the inner bore and the dedendum of the tooth.

Statistical analysis indicates that the standard deviation of effective strain increases from 0.25 to 0.26 as strain rate increases from 0.001 to 1 s^{-1} while temperature maintains at 250 °C. The reason lies in the fact that the flow stress increases with the increasing strain rate, as shown in Fig. 6. Thus, the friction between the billet and the die increases. For the region close to the inner bore of the gear and contacted with the flat end of the toothed punch, the friction hinders the development of deformation, so, the increase in friction force leads to the decrease in effective strain. Meanwhile, the friction contributes to metal filling for the tooth part of the gear, so, the increasing friction force leads to the increasing effective strain of this part. Therefore, the level of non-uniformity in effective strain distribution increases with increasing strain rate. As deformation temperature increases from 250 to 350 °C while strain

Table 1 Geometric parameters of gear

Teeth number	Module	Pressure angle/ (°)	Reference diameter/mm	Tooth thickness at reference diameter (Max/Min)/mm	Tip radius/mm	Bore diameter/mm
15	0.5812	14.5	8.7173	1.0668/1.0363	0.1143	3.985±0.01

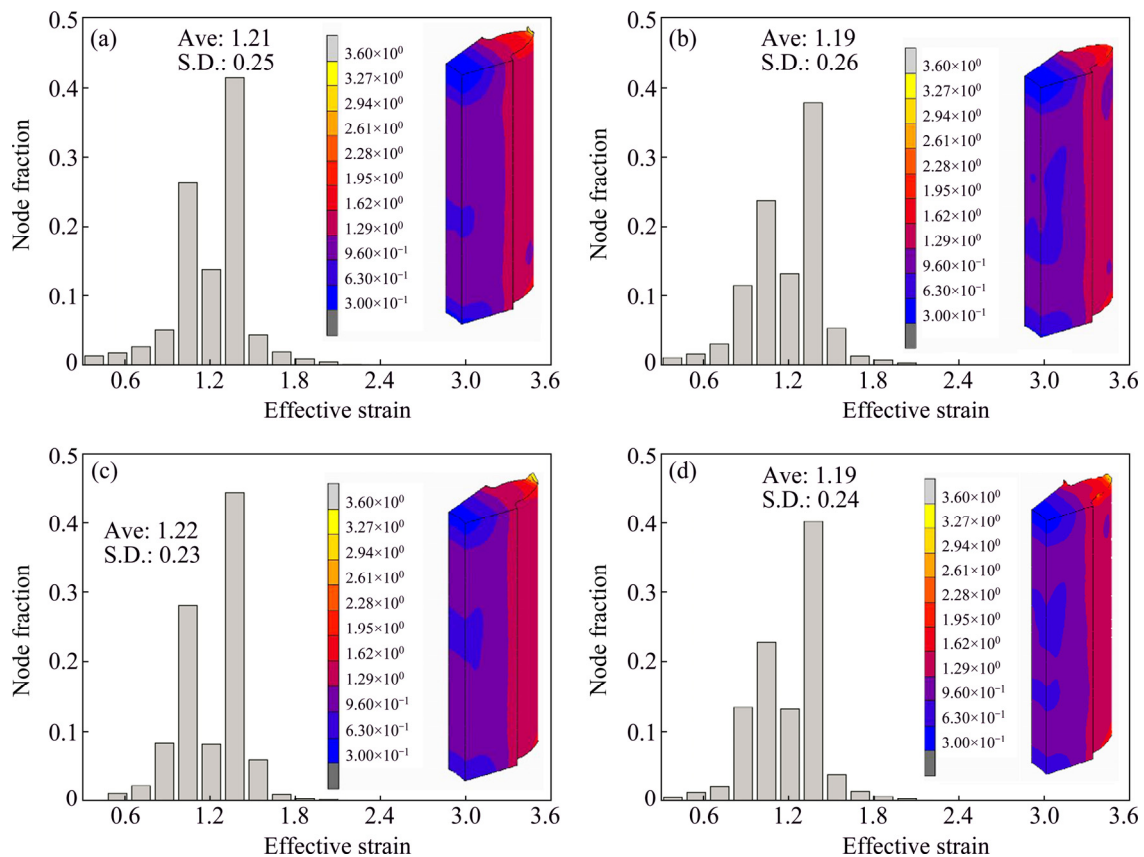


Fig. 5 Effects of deformation parameters on distribution of effective strain: (a) 250 °C, 0.001 s^{-1} ; (b) 250 °C, 1 s^{-1} ; (c) 350 °C, 0.001 s^{-1} ; (d) 350 °C, 1 s^{-1}

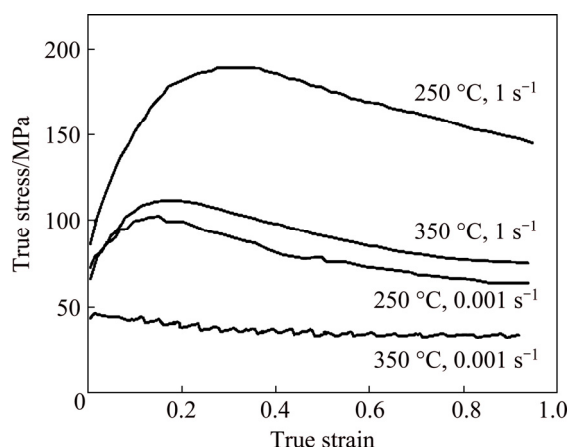


Fig. 6 Flow stress curves under different deformation conditions

rate maintains at 0.001 s^{-1} , standard deviation of effective strain decreases from 0.25 to 0.23, which indicates that the level of uniformity in deformation is improved as a result of decreasing flow stress.

Furthermore, the uniformity in the distribution of effective strain in the deformed gear is not only related to the flow stress but also associated with the shape of flow stress curve. In Fig. 6, flow stress curves of AZ31B magnesium alloys undergoing hot deformation show characteristics of dynamic recrystallization, that is, the true stress (deformation resistance) increases with increasing true strain at the beginning of deformation since work hardening plays a leading role at this stage; after the peak strain, the softening effect from dynamic recrystallization plays a dominant role, which results in the decrease of true stress as the true strain increases. When the spur gear is forged at temperature of $250 \text{ }^{\circ}\text{C}$ and strain rate of 1 s^{-1} , the effective strain at the area close to the inner bore and contacted with the flat end of toothed punch (the low-strain area) is much smaller than that at the other areas. At the low-strain area, the effective strain is about 0.34, where the flow stress is close to the peak value (Fig. 5(b) and Fig. 6). This indicates that high deformation resistance will impede the further deformation at the low-strain area; at the other areas, such as tooth tip, the effective strain is much greater than the peak strain and the flow stress is much smaller than the peak stress. As a result, further deform is easier to occur at high-strain area than that at low-strain area due to the significantly lowered deformation resistance. Therefore, the degree of non-uniformity in deformation for the gear forged at $250 \text{ }^{\circ}\text{C}$ and 1 s^{-1} is the largest one among the investigated four cases. As the spur gear is forged at $350 \text{ }^{\circ}\text{C}$ and 0.001 s^{-1} , the minimum value of effective strain at the end of forging is 0.45, which is much larger than the peak strain, but the flow stress does not vary significantly as compared with the

peak stress (Fig. 5(c) and Fig. 6). This means that there is no obvious difference in the ease of further deformation for the low-strain area and the high-strain area. As a result, the distribution of effective strain is more uniform than the other three cases.

3.2 Effects of deformation parameters on DRX fraction distribution

Figure 7 shows the simulated dynamic recrystallization (DRX) volume fraction of AZ31B spur gear upon the end of hot forging under the above four conditions. It can be found that under the condition with higher temperature and lower strain rate, dynamic recrystallization is more fully developed in the forged gear, the mean value of DRX fraction is larger and the standard deviation is smaller. At the temperature of $350 \text{ }^{\circ}\text{C}$ and strain rate of 0.001 s^{-1} , the dynamic recrystallization is fully developed. Statistics analysis shows that the DRX fraction of about 98.59% of the gear exceeds 95.00%. The mean value of DRX fraction is 99.80% and the standard deviation is only 0.01. By contrast, under the condition with low temperature and high strain rate, $250 \text{ }^{\circ}\text{C}$ and 1 s^{-1} , the development of DRX is rather uneven. The minimum value of DRX fraction is only 13.67% at the flat end of gear close to the inner bore, similar to the location of low-strain area. At the tooth part, the DRX fraction exceeds 91.31%. The mean value of DRX fraction is 90.64% and the standard deviation is 0.11. The non-uniformity in the DRX fraction is similar to that in the effective strain, which confirms that the development of DRX is closely associated with the level of deformation.

3.3 Effects of deformation parameters on average grain size distribution

Figure 8 shows the distribution of average grain size of AZ31B spur gears upon the end of the hot forging under above four different forging conditions. It can be seen that grain coarsening takes places at high temperature and low strain rate. Take $350 \text{ }^{\circ}\text{C}$ and 0.001 s^{-1} as an example, the average grain size is as large as $29.23 \text{ }\mu\text{m}$. Under the other three conditions, grain refining is observed and relatively coarse grain is obtained at the flat end of gear and close to the inner bore. When the strain rate increases from 0.001 to 1 s^{-1} at the temperature of $250 \text{ }^{\circ}\text{C}$, the average grain size decreases from 15.74 to $8.86 \text{ }\mu\text{m}$; however, the standard deviation of average grain size increases from 0.76 to $1.68 \text{ }\mu\text{m}$. This indicates that both the average grain size and the level of its uniformity decrease with increasing strain rate. This is because the accumulate rate of dislocation density increases with increasing strain rate. High dislocation density generates a large number of substructures due to the occurrence of dynamic recovery

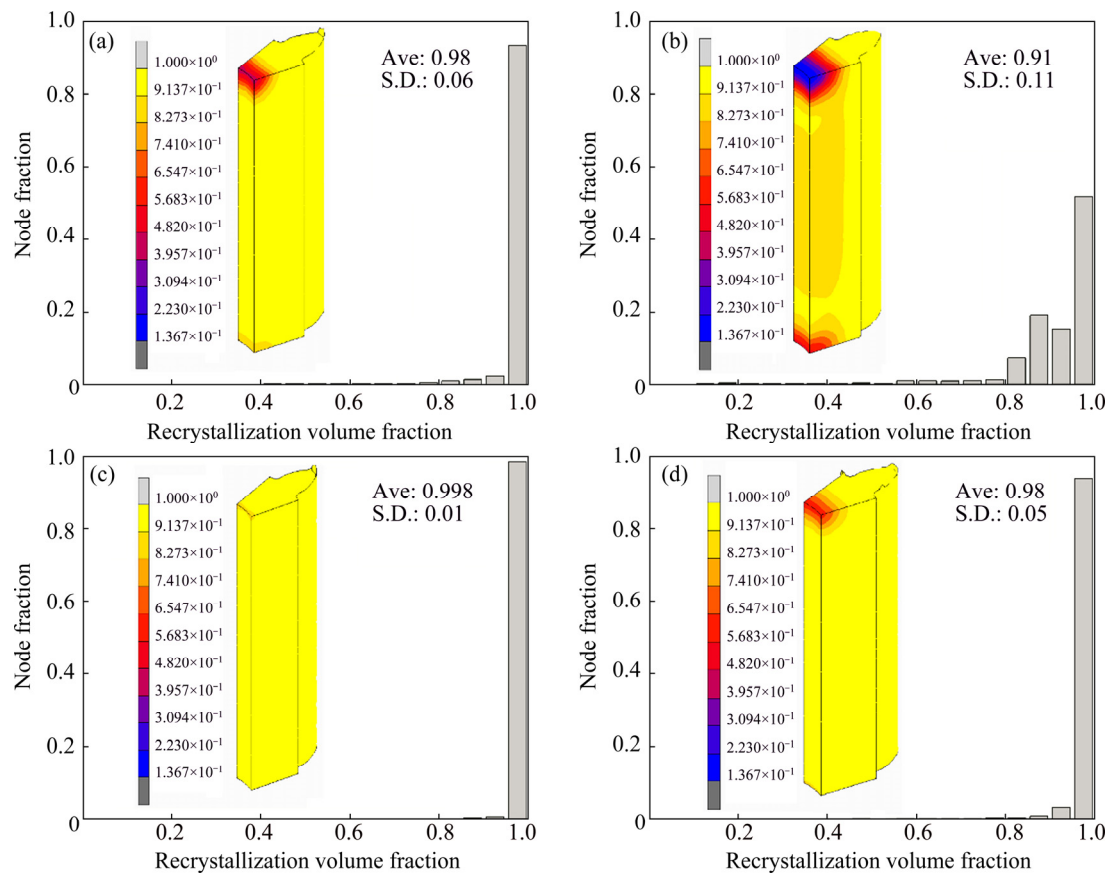


Fig. 7 Effects of deformation parameters on distribution of dynamic recrystallization fraction: (a) 250 °C, 0.001 s⁻¹; (b) 250 °C, 1 s⁻¹; (c) 350 °C, 0.001 s⁻¹; (d) 350 °C, 1 s⁻¹

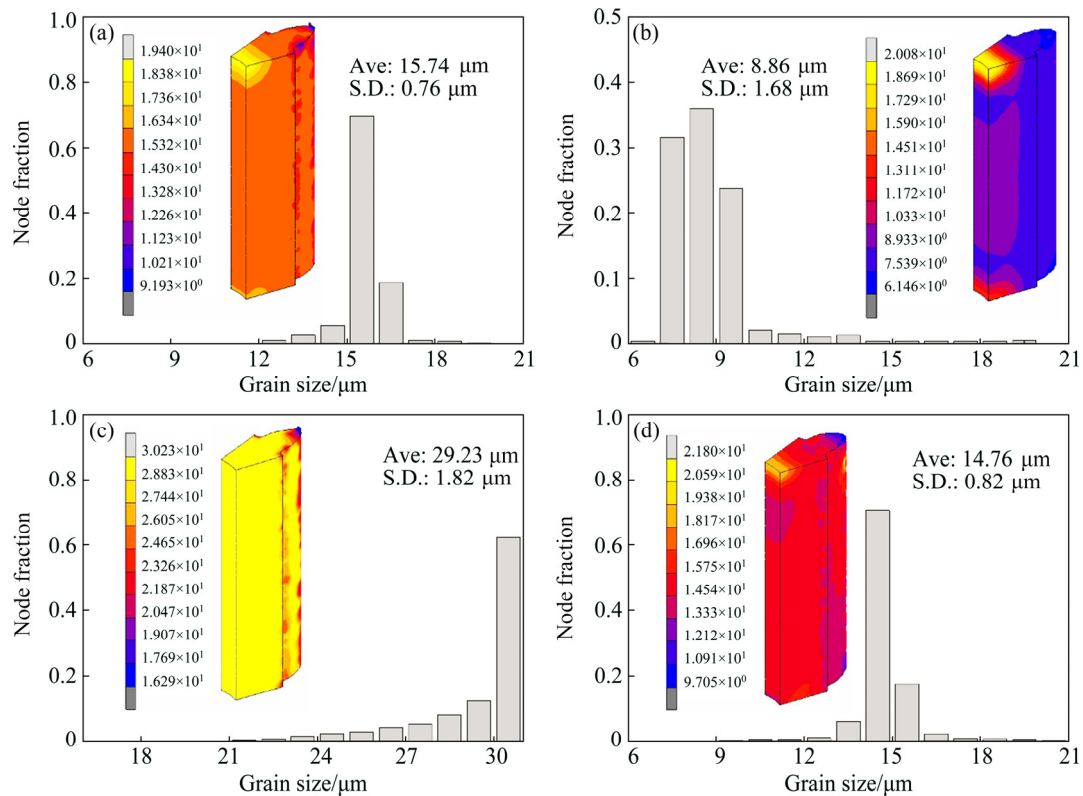


Fig. 8 Effects of deformation parameters on distribution of average grain size: (a) 250 °C, 0.001 s⁻¹; (b) 250 °C, 1 s⁻¹; (c) 350 °C, 0.001 s⁻¹; (d) 350 °C, 1 s⁻¹

and then produces a large number of DRX nuclei, which leads to fine-grained microstructure for the case of high-strain-rate deformation. But local average grain size in the deformed blocks depends on the local temperature, strain and strain rate. As shown in Fig. 2, the DRX fraction is lower at high strain rate or low strain if the temperature maintains constant. Thus, fine-grained microstructure is achieved in the large-strain area of the forged gear undergoing high-strain-rate deformation and relatively coarse grain in the low-strain area due to the insufficient development of DRX, which results in high level of non-uniformity in average grain size.

When the temperature increases from 250 to 350 °C as the strain rate keeps at 1 s^{-1} , the average grain size increases from 8.86 to 14.76 μm while the standard deviation decreases from 1.68 to 0.82 μm . With the increase of temperature, grain boundary mobility increases and thus the average grain size becomes coarser. Meanwhile, the critical strain for the initiation of DRX decreases and the DRX rate increases with increasing temperature as shown in Fig. 2. Thus, more fully developed recrystallization enhances the uniformity in average grain size.

4 Experiment verification

As discussed above, lower temperature or higher strain rate is beneficial to obtaining finer grains, but the

level of uniformity in grain size decreases at the same time. It is of great importance to optimize the processing parameters since fine and uniformly distributed microstructure contributes to excellent and uniformly distributed mechanical properties. Based on the numerical simulations in Section 3, a constant punch rate of 0.1 mm/s and a temperature of 300 °C were selected. Forging trials were carried out on a 100 kN electro-hydraulic servo testing machine. The billet was chosen as extruded tubes of AZ31B magnesium alloys. The mixture of butter and graphite was used as lubricant. To achieve the isothermal forging of AZ31B alloys, six heating rods, thermocouples and a customized temperature control device were connected with the designed die structure. The mixture of graphite and grease was used as lubricant to decrease the friction between the die and the billet.

Figure 9 shows the photograph of forged spur gear after removing burr and the simulated distribution of average grain size forged at 300 °C and 0.1 mm/s. It is shown that the forged gear was fully filled along the height of the tooth. According to the numerical simulation, the grain refinement is observed in most part of the gear except the area at the flat end of the gear and close to the inner bore where the average grain size is relatively coarse. Compared with the simulated results of the gear forged at 250 °C and 0.001 s^{-1} , which gives relatively fine grain and rather uniformly distributed

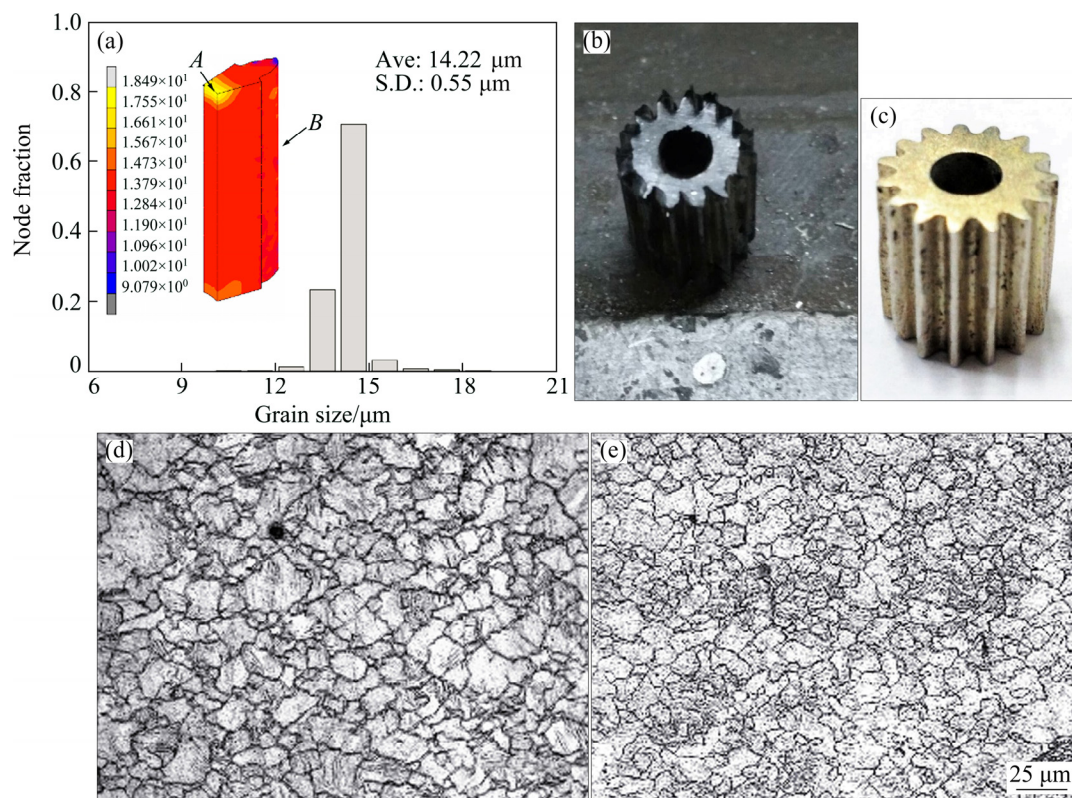


Fig. 9 Comparison between measured and simulated average grain sizes of gear forged at 300 °C and punch rate of 1 mm/s: (a) Simulated distribution of average grain size; (b) Photograph of forged gear with burr; (c) Photograph of forged gear after burr removal and cleaning; (d) Metallographic graph at characteristic point A; (e) Metallographic graph at characteristic point B

grain size as shown in Fig. 8(a), the average grain size under the trial condition reduces from 15.74 μm in Fig. 8(a) to 14.22 μm in Fig. 9(a), and the standard deviation of grain size decreases from 0.76 μm in Fig. 8(a) to 0.55 μm in Fig. 9(a). This indicates that forging under the chosen trial condition can provide fine-grained and rather uniform-distributed microstructure. In addition, time required for forging reduces significantly for the chosen trial condition.

In Fig. 9(b) and Fig. 9(c), the experimental metallographic morphologies at point *A* close to the inner bore and at point *B* at the tooth tip are also given for the ease of comparison. The average grain size at point *A* is 19.22 μm in Fig. 9(b), which is a bit larger than the simulated value of 18.49 μm . The average grain size at point *B* was measured as 14.33 μm in Fig. 9(c), which is also a bit larger than the simulated value of 13.87 μm . The well agreement between the simulated and measured results indicates that the thermal–mechanical microstructure coupled finite element model developed in this work is valid for predicting the microstructure evolution of hot forging process.

5 Conclusions

The thermal–mechanical microstructural coupled finite element model for AZ31B magnesium alloys is established and used for the precision forging process of straight spur gears. Both the numerical simulation and experimental examination show that straight spur gears with fully filled tooth can be achieved by using the movable cavity die design based on the friction-assistant principle. Either the deformation field or the average grain size is non-uniformly distributed in the as-forged gears. The non-uniformly distributed microstructure is closely associated with the non-uniform distribution of deformation, and the latter depends on the complex shape of spur gear on one hand, and on the contact friction between the billet and dies on the other hand. The friction force is related to the characteristics of flow stress curves, which is a function of forging parameters such as temperature, strain rate and strain. Statistics analysis shows that decreasing temperature or increasing strain rate is beneficial to obtaining fine-grained microstructure but the level of uniformity in grain size or in deformation becomes worse. Based on the numerical simulation, the temperature of 300 °C and constant punch rate of 0.1 mm/s were chosen to perform the trial forging. A fully filled gear with fine-grained microstructure and rather uniformly distributed grain size was achieved. Good agreement between the simulated and measured grain size validates the developed finite element model.

Acknowledgments

The authors gratefully acknowledge the helpful comments and suggestions made by Hong-biao DONG at the University of Leicester. Many thanks are also given to Jing BAI at Southeast University for his help in material preparation

References

- [1] TUNCER C, DEAN T A. Die design alternatives for precision forging hollow parts [J]. International Journal of Machine Tools & Manufacture, 1987, 27: 65–76.
- [2] SADEGHI M H, DEAN T A. Precision forging straight and helical spur gears [J]. Journal of Materials Processing Technology, 1994, 45: 25–30.
- [3] WANG Guang-chun, ZHAO Guo-qun, XIA Shi-sheng. New precision forging process and experimental study on spur gears [J]. Journal of Mechanical Engineering, 2005, 41: 123–126.
- [4] HU Cheng-liang, LIU Quan-kun, ZHAO Zhen, CHEN Jun, WU Gong-ming. Two step forging process of spur gear based on rigid parallel motion [J]. Journal of Shanghai Jiaotong University (Science), 2010, 15: 241–244.
- [5] ZUO Bin, WANG Bao-yu, LI Zhi, ZHENG Ming-nan, ZHU Xiao-xing. Design of relief-cavity in closed-precision forging of gears [J]. Journal of Central South University, 2015, 22: 1287–1297.
- [6] TAN Xian-feng, XIE Bao-hua, LIU Xia. Experiment and numerical simulation on precision forging for spur gear based on floating die and restrained split-flow [J]. Journal of Plasticity Engineering, 2016, 23: 7–10.
- [7] DONG Li-ying, LAN Jian, ZHUANG Wu-hao. Homogeneity of microstructure and Vickers hardness in cold closed-die forged spur-bevel gear of 20CrMnTi alloy [J]. Journal of Central South University, 2015, 22: 1595–1605.
- [8] ZHANG Xin-ming, FENG Di, SHI Xing-kuan, LIU Sheng-dan. Oxide distribution and microstructure in welding zones from porthole die extrusion [J]. Transactions of Nonferrous Metals Society of China, 2013, 23: 765–772.
- [9] WANG Cui-ju, DENG Kun-kun, ZHOU Shan-shan, LIANG Wei. Dynamic recrystallization behavior of bimodal size SiC_p -reinforced Mg matrix composite during hot deformation [J]. Acta Metallurgica Sinica (English Letters), 2016, 29: 527–537.
- [10] LI Xiao-cheng, DUAN Li-li, WU Xiao-chun. Experimental study and numerical simulation of dynamic recrystallization behavior of a micro-alloyed plastic mold steel [J]. Materials & Design, 2015, 66: 309–320.
- [11] LIU Juan, LI Ju-qiang, CUI Zhen-shan, RUAN Li-qun. A new one-parameter kinetics model of dynamic recrystallization and grain size predication [J]. Acta Metallurgica Sinica, 2012, 48(12): 1510–1519. (in Chinese)
- [12] QUAN Guo-zheng, PAN Jia, ZHANG Zhi-hua. Phase transformation and recrystallization kinetics in space–time domain during isothermal compressions for Ti–6Al–4V analyzed by multi-field and multi-scale coupling FEM [J]. Materials & Design, 2016, 94: 523–535.
- [13] CHEN Ming-song, LIN Y C, LI Kuo-kuo, ZHOU Ying. A new method to establish dynamic recrystallization kinetics model of a typical solution-treated Ni-based superalloy [J]. Computational Materials Science, 2016, 122: 150–158.
- [14] DANG Li, YANG He, GUO Liang-gang, SHI Lei, ZHANG Jun, ZHENG Wen-da. DRX rules during extrusion process of large-scale thick-walled Inconel 625 pipe by FE method [J]. Transactions of Nonferrous Metals Society of China, 2015, 25: 3037–3047.
- [15] WANG Sheng-long, YANG Bin, ZHANG Ming-xian, WU

- Huan-chun, PENG Jin-tao, GAO Yang. Numerical simulation and experimental verification of microstructure evolution in large forged pipe used for AP1000 nuclear power plants [J]. Annals of Nuclear Energy, 2016, 87: 176–185.
- [16] DING Han-lin, WANG Tian-yi, YANG Lei, KAMADO S. FEM modeling of dynamical recrystallization during multi-pass hot rolling of AM50 alloy and experimental verification [J]. Transactions of Nonferrous Metals Society of China, 2013, 23: 2678–2685.
- [17] JIN Zhao-yang, CUI Zhen-shan. Investigation on strain dependence of dynamic recrystallization behavior using an inverse analysis method [J]. Materials Science & Engineering A, 2010, 527: 3111–3119.

变形参数对 AZ31B 镁合金直齿圆柱齿轮热锻过程中变形和显微组织演变的影响

金朝阳¹, 李南南¹, 张琦¹, 严凯¹, 崔振山²

1. 扬州大学 机械工程学院, 扬州 225127;

2. 上海交通大学 国家模具 CAD 工程研究中心, 上海 200030

摘 要: 应用有限元模拟和统计分析方法研究变形参数对直齿圆柱齿轮成形过程中变形和显微组织演变的影响。将有限元方法与显微组织演化模型相集成建立了基于浮动凹模设计的齿轮成形有限元模型。采用 Gleeble 热力模拟实验和定量金相分析技术获得镁合金高温流动应力曲线和动态再结晶模型。数值模拟和实验检验表明, 由于齿轮形状复杂, 且坯料与模具间存在接触摩擦, 齿轮各部位变形和显微组织存在不均匀现象。变形温度降低或者变形速率增加, 有利于获得平均晶粒尺寸细小的组织, 但是变形和显微组织不均匀性增大, 其原因和流动应力曲线特征有关。

关键词: 镁合金; 直齿圆柱齿轮; 锻造成形; 有限元方法; 显微组织演变

(Edited by Xiang-qun LI)